Boundary-Layer Meteorol (2012) 144:83–112
DOI 10.1007/s10546-012-9715-8

ARTICLE

Towards a Validation of Scintillometer Measurements: The LITFASS-2009 Experiment

Frank Beyrich · Jens Bange · Oscar K. Hartogensis · Siegfried Raasch · Miranda Braam · Daniëlle van Dinther · Doreen Gräf · Bram van Kesteren · Aline C. van den Kroonenberg · Björn Maronga · Sabrina Martin · Arnold F. Moene

Received: 5 April 2011 / Accepted: 3 March 2012 / Published online: 28 March 2012

Abstract Scintillometry has been increasingly used over the last decade for the experimental determination of area-averaged turbulent fluxes at a horizontal scale of a few kilometres. Nevertheless, a number of assumptions in the scintillometer data processing and interpretation still call for a thorough evaluation, in particular over heterogeneous terrain. Moreover, a validation of the path-averaged structure parameters derived from scintillometer data (and forming the basis for the flux calculations) by independent measurements is still missing. To achieve this, the LITFASS-2009 field campaign has been performed around the Meteorological Observatory Lindenberg – Richard-Aßmann-Observatory of the

F. Beyrich (✉) · M. Braam · D. Gräf
Meteorologisches Observatorium Lindenberg, Richard-Aßmann-Observatorium, Deutscher Wetterdienst (DWD), Am Observatorium 12, 15848 Tauche - OT Lindenberg, Germany
e-mail: frank.beyrich@dwd.de

J. Bange · A. C. van den Kroonenberg
Zentrum für Angewandte Geowissenschaften (ZAG), Eberhard-Karls-Universität Tübingen, Sigwartstr. 10, 72076 Tübingen, Germany

M. Braam
Meteorology and Air Quality Group, Wageningen University and Research Centre, Droevendaalsesteeg 4, 6708 PB Wageningen, The Netherlands

O. K. Hartogensis · D. van Dinther · B. van Kesteren · A. F. Moene
Meteorology and Air Quality Group, Wageningen University and Research Centre, P.O. Box 47, 6700 AA Wageningen, The Netherlands

S. Raasch · B. Maronga
Institut für Meteorologie and Klimatologie, Fakultät für Mathematik und Physik, Leibniz-Universität Hannover, Herrenhäuser Str. 2, 30419 Hannover, Germany

Present Address:
A. C. van den Kroonenberg
Scintec AG, Wilhelm-Maybach-Strasse 14, 72108 Rottenburg, Germany

S. Martin
Institut für Luft- und Raumfahrt-Systeme, Technische Universität Carolo-Wilhelmina zu Braunschweig, Hermann-Blenk-Str. 23, 38108 Braunschweig, Germany

German Meteorological Service (DWD) in July 2009. The experiment combined tower-based in-situ turbulence measurements, field-scale laser scintillometers, long-range optical (large-aperture) and microwave scintillometers, and airborne turbulence measurements using an automatically operating unmanned aircraft. The paper describes the project design and strategy, and discusses first results. Daytime near-surface values of the temperature structure parameter, C_T^2, over different types of farmland differ by more than one order of magnitude in their dependence on the type and status of the vegetation. Considerable spatial variability in C_T^2 was also found along the flight legs at heights between 50 and 100 m. However, it appeared difficult to separate the effects of heterogeneity from the temporal variability of the turbulence fields. Aircraft measurements and scintillometer data agreed in magnitude with respect to the temporal variation of the path-averaged C_T^2 values during the diurnal cycle. The decrease of C_T^2 with height found from the scintillometer measurements close to the surface and at 43 m under daytime convective conditions corresponds to free-convection scaling, whereas the aircraft measurements at 54 and 83 m suggest a different behaviour.

Keywords Heterogeneous terrain · LITFASS · Scintillometer · Temperature structure parameter · Turbulence · Unmanned aircraft

1 Introduction

The turbulent exchange of momentum, energy and matter (e.g. of water vapour through evaporation, trace gases, aerosols etc.) is an essential element of land-surface–atmosphere interaction. The turbulent fluxes of sensible and latent heat exhibit a major influence on atmospheric processes such as boundary-layer growth, warming and moistening of the lower atmosphere, cloud formation and, consequently, precipitation patterns (e.g. Holtslag and Duynkerke 1998; Ek and Holtslag 2005). In numerical weather prediction (NWP) and climate numerical models the turbulent fluxes are described at a scale of 1–100 km (corresponding to the model grid resolution) using flux–profile relationships that relate the surface flux of a given quantity to its vertical gradient with an exchange coefficient as the factor of proportionality. Originally, these relations were derived from measurements performed over a locally homogeneous land surface (such as the grassland prairies in Kansas, USA, see e.g. Businger et al. 1971). In order to determine the local turbulent fluxes over homogeneous patches of the earth's surface, eddy-covariance techniques are the method of choice today (e.g. Lee et al. 2004). However, at the scale of several kilometres, the earth's surface is often strongly heterogeneous, as is the case in central Europe. Here, a model grid cell of 5–10 km side length typically contains patches of different types of farmland and forest, water, traffic roads, settlements etc. The local energy balance and hence the turbulent fluxes over these different types of underlying surface may differ considerably, even under comparable forcing conditions concerning precipitation and radiation. For example, during the LITFASS-2003 experiment a variability of a factor of 2–3 was found for the sensible heat flux between different types of farmland (grass, cereals, rape, maize) and also between a pine forest and the mean farmland flux (Beyrich et al. 2006; Bange et al. 2006b).

Techniques are therefore needed to provide area-averaged fluxes at the scale of a model grid cell. Different authors have shown that adequate averaging of flux values from local measurements over the main land-use classes (tile approach, e.g. Gryning et al. 2002; Beyrich et al. 2006) may provide reliable flux averages. But this method needs local flux measurements over all relevant types of land use; an alternative would be area-averaging flux measurement techniques. In the past, aircraft measurements have often been used for this purpose

Table 1 Typical values for the basic characteristic length scales of different scintillometer types

Parameter	DBSAS	LAS	MWS
Wavelength, λ	≈700 nm	850–950 nm	≈3 mm
Aperture diameter, D	(2.5 mm)	0.1–0.3 m	0.4 m
Beam separation, d	2.7 mm	–	–
Path height, h	0.5–10 m	10–50 m	10–50 m
Path length, L	50–200 m	0.5–5 km	0.5–10 km
First Fresnel zone diameter, F	≈10 mm	≈50 mm	≈5 m

(e.g. Mahrt et al. 2001; Bange et al. 2002a, 2006a,b; LeMone et al. 2007), which are, however, rather expensive and hence usually limited to case studies during special field experiments. Over the last 15 years, scintillometers have found increasing use as a relatively robust technique suited for the quasi-operational determination of at least the sensible heat flux. With a proper set-up, scintillometers may be operated over distances of several kilometres thus being able to provide turbulence parameters (and fluxes) at the scale of a grid box of a regional-scale NWP or climate model, or of the pixel of a satellite image (e.g. Watts et al. 2000; Lagouarde et al. 2002; Beyrich et al. 2002a; Chandrapala and Wimalasuriya 2003; Kleissl et al. 2009a).

Three different types of scintillometers have found broad interest in meteorological applications during the last decade, namely

- the (dual-beam) small aperture scintillometer (DBSAS),
- the (optical) large-aperture scintillometer (LAS), and
- the microwave scintillometer (MWS).

Typical values for the basic characteristics of these three scintillometer types are listed in Table 1.

The diameter of the first Fresnel zone, F, that is defined by $F = (\lambda L)^{1/2}$, and the aperture diameter, D, determine the size of the optically most active eddies that corresponds to the larger of the two. It becomes thus obvious from Table 1 that from a physical point of view the three scintillometer types differ in important characteristics.

The DBSAS is a small-aperture scintillometer with $D < F$, and is sensitive to eddy sizes of the order of 10 mm that are close to the inner scale length of turbulence, l_0. The DBSAS is typically used as a surface-layer scintillometer providing fluxes at the (micro-β) field scale. Heat fluxes derived from these measurements have been shown to compare well with local eddy-covariance measurements (e.g. Thiermann and Grassl 1992; Hartogensis et al. 2002; De Bruin et al. 2002; Hoedjes et al. 2002).

The LAS is a large-aperture scintillometer with $D > F$, implying that the LAS primarily "sees" eddies of the order of the aperture diameter of the optics that lie well within the inertial sub-range of the turbulence spectrum. LAS systems have been operated over distances of up to several kilometres (e.g. McAneney et al. 1995; Kohsiek et al. 2002; Asanuma and Iemoto 2007), and the derived path-integrated heat fluxes have been shown to compare well with independent estimates of area-averaged fluxes for a footprint area of several square kilometres. The potential of the LAS has been demonstrated for a variety of surface types from quasi-homogeneous (e.g. McAneney et al. 1995; De Bruin et al. 1995) to heterogeneous agricultural areas (e.g. Meijninger et al. 2002a; Lagouarde et al. 2002), different types of forest (e.g. Ezzahar et al. 2007a,b; Hoedjes et al. 2007), and mixed farmland–forest landscapes (Beyrich et al. 2002a) including valley sites (Meijninger and de Bruin 2000) and even urban areas (Lagouarde et al. 2006; Roth et al. 2006). Moreover, the LAS has been shown

to have the potential for continuous, unmanned long-term operation making it ideally suited for monitoring applications (Beyrich et al. 2002a).

For the MWS, $D < F$ holds and it therefore basically "sees" eddies with a size of F that still belongs to the inertial sub-range of the turbulence spectrum if the system is installed sufficiently high above the ground such that the outer scale of turbulence is larger than F. This outer scale represents the transition between the production range and the inertial sub-range in the spectrum of turbulence, and is of the order of magnitude of the measurement height. The fact that both the LAS and MWS are sensitive to structures in the inertial sub-range makes it possible to directly relate the measurements with these two types of systems. By combining optical and microwave scintillometers (MWSs) an estimation of the latent heat flux becomes possible in addition to the sensible heat flux—this has been demonstrated for a few case studies (e.g. Green et al. 2000, 2001; Meijninger et al. 2002b, 2006; Evans 2009). The simultaneous operation of a LAS and a MWS, but also the combination of a LAS with satellite data or hydrological models, offer additional perspectives with respect to water management studies at the regional scale (e.g. Chandrapala and Wimalasuriya 2003; Ezzahar et al. 2007b, 2009; Kleissl et al. 2009a; Cammalleri et al. 2010; Allen et al. 2011).

2 The Scintillometer Method—Achievements and Open Issues

2.1 Basic Principles

The scintillation technique is based on the propagation of electromagnetic radiation in the turbulent atmosphere. The energy of the electromagnetic radiation exhibits intensity fluctuations known as scintillations that are caused by fluctuations of the refractive index n of the air within the propagation beam. The magnitude of these fluctuations can be expressed by the refractive-index structure parameter, C_n^2, which is the basic parameter derived from scintillometer measurements. It can be derived from the variance of the logarithm of the signal amplitude, B_i, measured at the receiver side of a scintillometer system (with equal aperture diameters for the transmitter and receiver):

$$B_i = 16\,\pi^2 k_\lambda^2 \int_0^L dx \int_0^\infty d\kappa\ \phi_n(\kappa, l_0, C_n^2)\ \sin^2\left[\frac{\kappa^2 x(L-x)}{2k_\lambda L}\right]\left[\frac{4J_1^2(\kappa Dx/2L)}{(\kappa Dx/2L)^2}\right], \quad (1)$$

where k_λ is the optical wavenumber, κ is the turbulent spatial wavenumber, ϕ_n is the three-dimensional spectrum of refractive index, l_0 is the inner-scale length of turbulence, D is the aperture diameter, L is the path length, x is the distance along the path and J_1 is a Bessel function of the first kind.

Within the inertial sub-range and for the conditions of locally isotropic turbulence, the structure parameter of any given atmospheric quantity, X, is defined as (e.g. Tatarskii 1961):

$$C_X^2 = \left\langle (X(\boldsymbol{r}_1) - X(\boldsymbol{r}_2))^2 \right\rangle\ r^{-2/3}, \quad (2)$$

where $r = |\boldsymbol{r}_1 - \boldsymbol{r}_2|$ is the spatial separation between two points $\boldsymbol{r}_1$ and $\boldsymbol{r}_2$, and the angle brackets denote an ensemble average. X may represent temperature, T, humidity, q, refractive index, n, or wind velocity, $\boldsymbol{v}$. In analogy, the co-structure parameter between two quantities (X, Y) can be defined as the correlation product between $X(\boldsymbol{r}_1) - X(\boldsymbol{r}_2)$ and $Y(\boldsymbol{r}_1) - Y(\boldsymbol{r}_2)$. Direct application of Eq. 2 requires measurements of the quantity of interest at two points

separated by some distance r within the inertial sub-range. If the Taylor hypothesis of frozen turbulence is applicable, C_X^2 may also be derived from single-point measurements (e.g. Kohsiek 1982):

$$C_X^2 = \left\langle (X(t_1) - X(t_2))^2 \right\rangle (\Delta t V)^{-2/3}, \tag{3}$$

where V is the mean wind speed, and t_1 and t_2 are two time instants separated by Δt.

The refractive-index structure parameter, C_n^2, can be related to the meteorological structure parameters C_T^2, C_q^2, and C_{Tq} via (e.g. Hill et al. 1980):

$$C_n^2 = \frac{A_\mathrm{T}^2}{T^2} C_T^2 + \frac{2A_\mathrm{T}A_\mathrm{q}}{Tq} C_{Tq} + \frac{A_\mathrm{q}^2}{q^2} C_q^2. \tag{4}$$

Here, A_T and A_q are functions representing the partial derivatives of refractive index versus temperature and humidity, respectively; these functions depend on temperature, humidity, air pressure and on the electromagnetic wavelength. The pressure dependence is only weak and can be neglected to a first approximation.

For optical wavelengths (visible and near-infrared) the first term dominates but the second term can not be completely neglected; the last term is small. A practical approach to account for the humidity contribution to C_n^2 has been suggested by Wesely (1976):

$$C_T^2 = C_n^2 \frac{T^2}{A_\mathrm{T}^2} \left(1 + \frac{0.03}{Bo}\right)^{-2}, \tag{5}$$

where Bo is the Bowen ratio. The constant 0.03 in Eq. 5 was derived for $T = 300\,\mathrm{K}$, $p = 1,000\,\mathrm{hPa}$ and assuming a correlation coefficient between T and q in the inertial sub-range $r_{Tq} = \pm 1$. This equation has been used in many studies to derive the sensible heat flux from measurements with an optical large aperture scintillometer (e.g. Beyrich et al. 2002a; Meijninger et al. 2002a; Kleissl et al. 2008).

For wavelengths on the scale of millimetres the third term in Eq. 4 dominates, while the absolute value of the second term is about 10 % of the third and is of opposite sign. The first term is the smallest but cannot be fully neglected. Expressions for A_T and A_q in the infrared and microwave range are given, e.g. in Hill et al. (1980) and Andreas (1989). Moene (2003) showed that a good approximation for C_{Tq} is

$$C_{Tq} = r_{Tq} \sqrt{C_T^2 C_q^2}. \tag{6}$$

It can be inferred from Eq. 4 that C_T^2 and C_q^2 can be evaluated from the measurements of C_n^2 at two different wavelengths provided that r_{Tq} is known.

Derivation of the turbulent flux of sensible heat from scintillometer measurements is based on the application of Monin-Obukhov similarity theory (MOST) using the following similarity relationship for the vertical profile of the temperature structure parameter (e.g. Hill 1997):

$$\frac{C_T^2 (z-d)^{2/3}}{T_*^2} = f_\mathrm{T}\left(\frac{z-d}{L}\right), \tag{7}$$

where f_T is a universal function of $(z-d)/L$, z is the (effective) height of the scintillometer beam, and d is the zero-plane displacement. The Obukhov length is defined as $L = u_*^2 T/(g\kappa T_*)$ where u_* is friction velocity, $T_* = -\langle w'T' \rangle / u_*$ is the temperature scale, $\langle w'T' \rangle$ is the kinematic heat flux, κ is the von Kármán constant, and g is the acceleration due to gravity. An analogous equation can be formulated for the profile of the humidity structure parameter that is then used to derive the latent heat flux.

2.2 Open Issues

Although scintillometers have been successfully applied in numerous studies to determine area-averaged heat fluxes at the kilometre scale, there are still a number of open issues that require further research. Some of these issues are briefly discussed in the following paragraphs.

2.2.1 Similarity Functions

There is still no unanimity in the literature on the mathematical form of the universal functions f_T and f_q, and different formulations have been suggested (e.g. Wyngaard et al. 1971; Foken and Kretschmer 1990; Thiermann and Grassl 1992; De Bruin et al. 1993; Hartogensis and De Bruin 2005). Meijninger et al. (2006) discussed the uncertainty range introduced by the use of different functions on the resulting fluxes that may be of the order of 10–15 %. For variances the possible impact of the inequality of the universal functions for temperature and humidity has received attention (e.g. De Bruin et al. 1993, 1999; Moene et al. 2006a,c), but possible consequences on scintillometer-based fluxes have not been investigated to date. In all scintillometry studies these functions have been taken as equal, i.e., $f_T = f_q$, and moreover, these similarity functions are strictly valid for the surface layer only. However, in scintillometer data analysis they are usually applied to measurement heights of several decametres above the ground. This appears to be justified under convective conditions where surface-layer scaling of structure parameters has been found to hold for the lower part of the mixed layer as well (e.g. Kohsiek et al. 2002). In contrast, under stable conditions significant deviations from surface-layer scaling have to be considered even at a few decametres above the surface and no universal scaling law has been found so far for the bulk of the stable boundary layer (e.g. Wyngaard and Kosovic 1994). The application limits of surface-layer similarity scaling to scintillometer measurements above the surface layer, especially under stable conditions, has not been thoroughly assessed to date.

2.2.2 Heterogeneous Terrain

Theoretically, the application of similarity methods should be restricted to homogeneous surfaces, and its use over heterogeneous surfaces requires the existence of a 'blending height' somewhere below the scintillometer path. This assumption might be justified over mixed agricultural surfaces (e.g. Meijninger et al. 2002a,b) where the signatures of different patches of farmland with a typical size of less than 1 km^2 can be expected to vanish at a few decametres above the ground. Otherwise a careful footprint analysis would be necessary in order to relate the scintillometer signal to the different patches from which the turbulence signals along the path originate (e.g. Meijninger et al. 2006). The existence of a blending height for fluxes is still debated controversially, especially over moderately heterogeneous terrain (e.g. Bange et al. 2006b). No studies at all are known to the authors dealing with the question of identifying a blending height for structure parameters. When performing an averaging over the local measurements at different patches in the footprint area of a scintillometer it has to be noted that the relation between the structure parameters and the fluxes is non-linear, hence different results are obtained depending on whether the averaging is performed for fluxes or for structure parameters. For the latent heat flux this difference may be of the order of 10-15 % (Meijninger et al. 2006). Aggregation rules for structure parameters have still to be developed and validated. Flux aggregation over heterogeneous terrain is also relevant for the

determination of the Bowen ratio that enters the correction term in Eq. 5, and which has to be applied to transform C_n^2 into C_T^2 if the sensible heat flux is determined from single-wavelength LAS measurements.

2.2.3 Independent Validation of the Scintillometer Principle

A validation of scintillometer measurements has been performed in most cases by comparing the scintillometer-based fluxes against flux values derived from (aggregated) in-situ eddy-covariance measurements (e.g. Meijninger et al. 2002a,b, 2006). Beyrich et al. (2005) performed an evaluation of the structure parameters derived from scintillometer measurements against tower-based in-situ turbulence measurements using a sonic anemometer-thermometer and a fast-response hygrometer, but this represents a comparison of point measurements versus path-integrated values. In a few studies airborne measurements have been considered for comparison, but these were usually representative of a larger area (e.g. Moene et al. 2006b; Beyrich et al. 2006) than that covered by the scintillometer path. Thus, no validation of the path-integrated structure parameters from scintillometer measurements against independent data representative just for the scintillometer path from either airborne measurements or model results has become known so far.

2.2.4 The Bi-Chromatic Technique

By combining optical and MWSs, estimation of the latent heat flux becomes possible in addition to the sensible heat flux—this has been demonstrated for a few case studies (e.g. Green et al. 2000, 2001; Meijninger et al. 2002b, 2006). In order to determine C_T^2, C_q^2, and C_{Tq} from LAS–MWS measurements, these authors have used the so-called "two-wavelength method" (e.g. Kohsiek and Herben 1983; Andreas 1989). With this method, path-averaged values of the refractive-index structure parameter ($C_{n1}^2 = C_n^2(\lambda_1)$, $C_{n2}^2 = C_n^2(\lambda_2)$) are derived from simultaneous measurements at two different wavelengths, λ_i, one in the optical, λ_1, and one in the microwave, λ_2, range of the electromagnetic spectrum. Taking into account that C_n^2 is a function of the three "meteorological" structure parameters (see Eq. 4), measurements at two wavelengths are not sufficient to close the resulting equation system. This would call for a "three-wavelength method" that was discussed by, e.g., Hill et al. (1988), but it has never been realized successfully in an experiment. Instead it is usually assumed that temperature and humidity fluctuations are perfectly correlated (either positive or negative, $r_{Tq} = \pm 1$), which implies $C_{Tq} = \pm(C_T^2 C_q^2)^{1/2}$ (see Eq. 6). To avoid this assumption, Meijninger et al. (2006) have used eddy-covariance measurements of r_{Tq} (which however represent a point measurement in relation to the size of the LAS–MWS path of several kilometres) in order to calculate C_{Tq} from Eq. 6. Lüdi et al. (2005) have for the first time measured the correlation between optical and microwave scintillations allowing for a direct estimation of C_{Tq} (and also of the temperature-humidity correlation, r_{Tq}) from scintillometer data. This so-called 'bi-chromatic' technique has several advantages, in addition to the estimation of the path-averaged C_{Tq} from the measurements without the assumption of $r_{Tq} = \pm 1$ it also gives the sign of r_{Tq}. The bi-chromatic technique (direct measurements of the correlation between optical and microwave scintillations) has not been thoroughly evaluated yet with respect to the effects of saturation and different path weighting functions of its optical and microwave components.

2.2.5 Tower Vibrations

Application of scintillometers at the meso-γ (grid) scale requires measurements over distances of several kilometres. For such path lengths, signal saturation may occur in case of intense turbulence (e.g. Kohsiek et al. 2006). In order to avoid saturation the transmitter and receiver units have to be mounted at heights of several decametres above ground which is often achieved by using lattice masts as a mounting structure. However, these masts are normally subject to wind-induced vibrations that might affect the scintillation measurements. In analyzing the scintillometer data from the LITFASS-2003 experiment, Beyrich et al. (2005) and Meijninger et al. (2006) found that the MWS measurements were affected by tower vibrations if the wind speed at the scintillometer level was >6–$7\,\mathrm{m\,s^{-1}}$, and they had to exclude the strong-wind cases from their analysis. Von Randow et al. (2008) report about vibration effects on LAS measurements performed at two tall lattice towers above the Amazonian rain forest. They corrected the LAS measurements by fitting their data with a theoretical model spectrum. However, apart from such an empirical diagnosis of vibration effects on scintillometer measurements, a detailed analysis of the influence of tower vibrations on scintillation measurements based on a direct measurement of these vibrations has not been described in the literature to our knowledge.

2.2.6 Friction Velocity

For daytime convective conditions the influence of u_* on the derived fluxes (via L in Eq. 7) is relatively small (e.g. De Bruin et al. 1995). Thus a crude estimate of friction velocity based on wind-speed measurements at a single level suffices to account for it. Over tall rough vegetation (forest) or over a heterogeneous landscape and during stable conditions this is no longer valid. However, algorithms for flux estimation from scintillometer data generally use friction velocity estimates from point measurements that are not a-priori representative of the scintillometer path.

3 The LITFASS-2009 Experiment

3.1 The Measurement Strategy

To further substantiate the application of scintillometers an experiment has been designed to collect data that could contribute to answering the open issues discussed in Sect. 2.2. This experiment was performed in the area around the Meteorological Observatory Lindenberg – Richard-Aßmann-Observatory (MOL-RAO) of the Deutscher Wetterdienst (DWD, German Meteorological Service), the so-called LITFASS area. The acronym LITFASS stands for Lindenberg Inhomogeneous Terrain – Fluxes between the Atmosphere and the Surface: a longterm Study, and represents a program to study the question of the area averaging of turbulent fluxes over the heterogeneous land surface around the MOL-RAO with respect to the application to NWP modelling. This program includes the operational boundary-layer measurement activities at MOL-RAO and also a series of field experiments performed in the area (Neisser et al. 2002; Beyrich et al. 2002b; Beyrich and Mengelkamp 2006). In the present context, LITFASS might also be understood as LIndenberg-To-Falkenberg Aircraft Scintillometer Study. The LITFASS-2009 experiment took place from June 29 to July 24, 2009.

Table 2 Measurement strategy with respect to the research topics from Sect. 2.2

Issue	Measurements
Similarity functions	Combination of surface-layer, tower based and airborne turbulence measurements using eddy-covariance techniques
Heterogeneous terrain	Surface-layer scintillometer measurements of structure parameters over all relevant patches of land use along the LAS path
	Profile measurements of structure parameters along a tower, with aircraft and LAS at different heights
Scintillometer validation	Airborne measurements of structure parameters along the LAS path
Bi-chromatic technique	Parallel LAS and MWS measurements with high-frequency (> 100 Hz) sampling of the raw data
Tower vibrations	Acceleration measurements in combination with the scintillometer measurements at high sampling frequency
Friction velocity	Path-averaged wind measurements using a scintillometer with cross-wind capability
	Airborne wind and turbulence measurements along the LAS path

The general ideas with respect to the measurement strategy of this experiment are summarized in Table 2.

3.2 Site Conditions

A map of the area around Lindenberg/Falkenberg with the land use during summer 2009 indicated is presented in Fig. 1. The landscape in the region around MOL-RAO has been formed by the inland glaciers of the last ice age. It is characterized by moderate changes in orography (terrain height varies between about 40 and about 130 m above sea level over an area of $25 \times 25\,\mathrm{km}^2$), and it represents a mixture of forest and farmland with small and medium-sized lakes embedded. A number of small villages (each with a few hundreds of inhabitants typically) is spread over the region at typical distances of about 3–5 km.

MOL-RAO operates two facilities in this area: the observatory site and a special boundary-layer field site, the so-called GM Falkenberg (where GM stands for "Grenzschichtmessfeld", the German translation of "boundary-layer field site"). Both sites are about 5 km apart from each other. At the observatory site, a suite of ground-based remote sensing systems (including wind profiler radar, microwave profiler radiometer, cloud radar, ceilometer), a radiosonde station (with four regular launches per day), and a platform for measurements of broadband and spectral downward radiation components are in routine operation. At the GM Falkenberg measurements of meteorological parameters are performed at various masts and towers (up to a height of 98 m) providing a detailed characterization of micrometeorological processes including soil physical parameters, profiles of mean atmospheric state variables, radiation and turbulent energy fluxes. A sodar-RASS system is used to measure wind and temperature profiles beyond the tower range. A LAS has been in operation over the 4.9 km distance between the two sites for more than 10 years providing the background measurements for the LITFASS-2009 field experiment.

A footprint analysis for the LAS path has been performed by Meijninger et al. (2006). It revealed that more than 90 % of the turbulent signal at the height of the LAS beam can be attributed to the different agricultural fields below and around the path, except for the wind

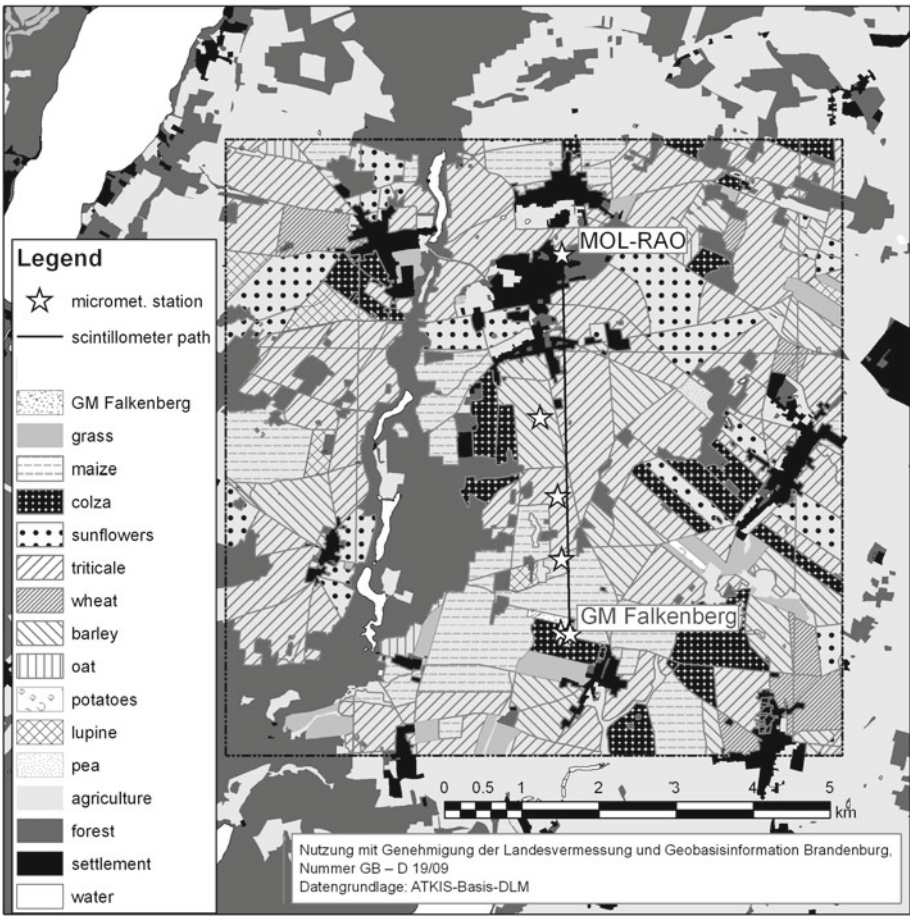

Fig. 1 Map of the study region around the MOL-RAO: the LAS path and the positions of the micrometeorological ground stations—see Sect. 3.3—are marked by the *line* and *star symbols*, respectively

direction sector around west for which about 10–15 % of the signal may result from the forest patches visible in Fig. 1.

3.3 Measurement Systems

In addition to the operational measurement systems at MOL-RAO the following instruments have been employed during LITFASS-2009. Five micrometeorological stations were set up over different agricultural fields to perform surface-layer measurements of mean meteorological quantities, energy fluxes and turbulence parameters over the major types of farmland: grass, triticale, barley, maize, and colza. Turbulence measurements at these stations were carried out using USA-1 (METEK GmbH, Germany) or CSAT-3 (Campbell Sci., UK) ultrasonic anemometers/thermometers and LI-7500 (LiCor Inc., U.S.) infrared hygrometers. Five dual-beam surface-layer scintillometers (SLS-20/SLS-40, manufactured by Scintec AG, Germany) were operated close to the micrometeorological field stations. These instruments provided surface-layer measurements of the refractive-index structure parameter

Table 3 Set-up characteristics of the surface-layer turbulence measurements

	Grass (Colza)	Colza (Grass)	Maize	Barley	Triticale
Eddy covariance					
Sonic	USA-1	USA-1	USA-1	CSAT-3	CSAT-3
Hygrometer	LI7500	LI7500	LI7500	LI7500	LI7500
Height (m)	2.4	2.4	5.2	3.2	3.2
Scintillometer					
Type	SLS-40	SLS-40	SLS-20	SLS-20	SLS-20
Orientation	south → north	north → south	west → east	east → west	north-east→ south-west
Path height (m)	2.15	2.4	2.40	2.31	2.35
Pathlength (m)	125	117	125	120	110

representative of the different farmland types. Two eddy-covariance stations and two SLS-40 systems were installed at the eastern and western borders of the GM Falkenberg field site, respectively. Depending on the actual wind direction, these sensor systems "saw" in their footprint area either the grassland of the field site or the colza at the neighbouring fields. A summary characterizing the operating conditions of the eddy-covariance and scintillometer systems at the five field stations is given in Table 3.

Two more eddy-covariance systems (combining a USA-1 with a LI-7500) were mounted at the 50- and 90-m levels of the meteorological tower at GM Falkenberg. The instruments were installed on the booms pointing towards 190° at a distance of about 4 m from the mast construction. This allowed for turbulence measurements not significantly affected by the tower itself for wind directions between 090° and 300°. Temperature, wind and humidity fluctuations were measured at a sampling rate of 20 Hz. Tower and boom accelerations in three directions were measured with the same frequency using BG-2168 accelerometers (M+S GmbH, Germany).

In addition to the operational LAS, a second LAS and two MWS were installed at the GM Falkenberg and MOL-RAO towers. Both LAS systems (abbreviated as LASDWD and LASWUR below) were built at the University of Wageningen (The Netherlands, Meijninger et al. 2000; Moene et al. 2005), they have an aperture of 0.152 m, the operating wavelength is 940 nm. The MWS systems were built at the University of Bern (Switzerland, e.g. Lüdi et al. 2005) and Rutherford Appleton Laboratory (UK, e.g. Evans 2009), respectively (we call them the MWUB and MWRAL systems). Both are operated at 94 GHz (3 mm wavelength), the apertures are 0.4 and 0.25 m, respectively. BG-2168 accelerometers were attached to the scintillometer units at both the Falkenberg and Lindenberg towers. A combined storage of the raw data from the LAS and MWS systems (including the accelerometers) has been realized at 500 Hz sampling frequency.

Airborne measurements were performed using the M^2AV (meteorological mini aerial vehicle) research aircraft, developed at the Technische Universität (TU) Braunschweig. M^2AV is an electrically powered, twin-engined aeroplane that operates automatically, i.e., without remote control. It is controlled by an on-board autopilot system that communicates with a ground station (laptop PC) for the exchange of measured data and mission updates, e.g. new waypoints. The aircraft has a take-off weight of 6 kg (including 1 kg of payload) and a wing span of 2 m. It is equipped with temperature and wind vector sensors for turbulence measurements (up to 0.033 s time resolution), a humidity sensor (1 s) and a sophisticated navigation

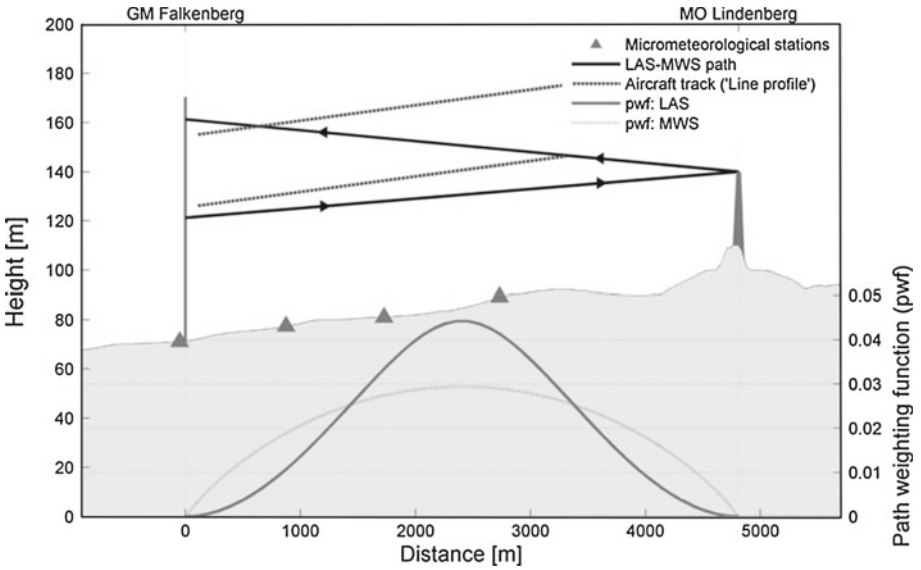

Fig. 2 Schematic cross-section of the measurement set-up along the Falkenberg-to-Lindenberg LAS–MWS path. *Grey-shading marks* the terrain height, and the pwf of the LAS and MWS are indicated in the lower part of the figure. The micrometeorological stations represent grass/colza, maize, triticale, and barley from *left to right* (south to north), respectively

and attitude measurement system. All data are recorded at 100 Hz sampling frequency. At a 22 m s^{-1} air speed a spatial resolution in the sub-metre range is achieved. More comprehensive information is given in Spieß et al. (2007), van den Kroonenberg et al. (2008), and Martin et al. (2011).

3.4 Experimental Set-up

The general experimental set-up in the area around the MOL-RAO and GM Falkenberg can be inferred from Fig. 1. The LAS–MWS path extends over a distance of 4.9 km between the two sites, and the five micrometeorological stations and the laser scintillometers were installed at four fields along the LAS–MWS path. Two stations were operated at the eastern and western borders of the GM Falkenberg that was surrounded by colza fields in 2009. Measurements with these two stations thus represented the conditions over grassland and over colza with a dependence on the prevailing wind direction. Figure 2 shows a schematic x–z cross-section along the LAS–MWS path (that was almost oriented south-north).

The terrain height slightly increases along the path. The two LAS–MWS systems employed during LITFASS-2009 were set up for an anti-parallel operation. The transmitters of the LAS-DWD–MWUB system were mounted at the 50-m level of the Falkenberg tower (123 m above sea level) while the receivers were installed at the upper platform (25 m, corresponding to 133 m above sea level) of a tower at the observatory site. The LASWUR–MWRAL system had its transmitters at this location, while the receivers were mounted at the 90-m level of the Falkenberg tower. The measurements with the two systems thus represented two different effective heights above ground (about 43 and 63 m, respectively). The lower path was almost parallel to the surface except for the parts close to the receiver site.

Two different flight patterns were defined for the operation of the M^2AV aircraft during the experiment. The first pattern consisted of straight legs at different heights along the path but parallel to the surface ("Line profile"). Alternatively the aircraft followed the height of the scintillometer beams along the path ("Scintillometer profile"). Unfortunately, the flight legs had to end at round 3.3 km north of the Falkenberg tower (thus covering about 70 % of the LAS–MWS path) since we did not have permission to fly above the village of Lindenberg.

The path-weighting functions (pwf) for the two scintillometers are also shown in Fig. 2; they indicate that the major contribution to the receiver signal arises from a region around the centre of the path, in particular for the LAS.

3.5 The Meteorological Conditions

The meteorological conditions during the LITFASS-2009 experiment were not very favourable with respect to the project goals. At the beginning of the experiment, the weather was characterized by weak synoptic pressure gradients over Germany, while showers and thunderstorms frequently developed within the prevailing humid and unstable air masses. The last two weeks of the experiment were characterized by a cyclonic westerly to south-westerly flow with frequent passages of low pressure systems and associated precipitation. Cloudless conditions never lasted longer than a few hours, the daily sum of sunshine duration exceeded 8 h on five days only during the measurement period (when the maximum possible sunshine duration was about 15 h). Rain occurred on 17 out of the 26 days of the field campaign. The wind speed at 10 m during the daytime frequently exceeded $6\,\mathrm{m\,s^{-1}}$ with considerable gustiness preventing a safe operation of the M^2AV aircraft. As a consequence, measurement flights were often possible (and reasonable) during certain hours of the day only. During the whole measurement period, 16 flights were performed on six days along the "Line profile" and "Scintillometer profile" patterns described above.

3.6 DBSAS Inter-Comparison Experiment

As a pre-requisite for the interpretation of possible differences in the C_T^2 measurements at field scale derived from DBSAS measurements over different surface types a quantification of the instrumental uncertainty (i. e., the differences obtained when operating the systems over the same type of surface) is necessary. So far, only a few scintillometer comparison results have been published in the scientific literature (e. g., Kleissl et al. 2008, 2009b; van Kesteren and Hartogensis 2011), and mainly consider the commercially available LAS systems from Scintec and Kipp&Zonen. Moreover, published results generally focus on the derived fluxes. We are not aware of any publication on the comparison of a number of DBSAS with respect to the basic meteorological output variables, namely C_n^2 and l_0. Before installing the SLS-20/40 systems at the agricultural fields we therefore performed a 3-day inter-comparison experiment at the GM Falkenberg grassland site. The five DBSAS were set up over a path-length of 145 m and at a measurement height of 2.15 m. The orientation of the paths was roughly east-west with prevailing northerly winds predicted for the period of the comparison experiment. The lateral distance between four of the paths was 8–10 m, for logistic reasons the fifth path was about 40 m to the north of the fourth path. The diagnosis data period was set to 6 s and the basic averaging interval was set to 10 min for the measurements during this experiment. All five paths "saw" the grass at GM Falkenberg over a fetch of at least 150 m. Since the upstream, along-wind footprint area of a measurement system installed at 2 m or higher extends over several tens of metres, the source areas for the different paths largely overlap for the lateral distance we have used in this set-up.

4 Data Processing

Most of the measurements made during LITFASS-2009 were focused on the determination of the temperature structure parameter, C_T^2. This can be obtained from optical scintillometer measurements, while derivation of the humidity structure parameter, C_q^2, has to rely on combined LAS–MWS measurements. Moreover, a lightweight, fast-response humidity sensor suitable for installation on the M^2AV aircraft was not available at the time of the experiment. The description of the data processing and the presentation of results will therefore basically concentrate on C_T^2.

4.1 Structure Parameters from the DBSAS Data

Determination of the structure parameters from the DBSAS data was based on the SLS-Run/SRun system software provided by the manufacturer. This software determines C_n^2 from the variances and from the covariance of the logarithmic intensity of the received signals of two parallel laser beams. The inner scale length of turbulence l_0 is derived from the correlation of the signal intensity between the two beams. Internal analysis of the signal is performed over so-called diagnosis intervals (the length of which was set as 10 s). A series of statistical tests is internally applied to the signals during one diagnosis interval, and an error code is assigned to the 10 s dataset based on the results of these tests (where error_code = 0 indicates that all tests have been passed). Statistics from the single sampling periods are then aggregated to 10-min averages of the derived parameters whereby only data from sampling intervals without an error message are considered. C_T^2 was then calculated from C_n^2 using Eq. 5. The Bowen ratio, *Bo*, was determined from the flux measurements of the eddy-covariance systems at the five sites, and mean values of *Bo* over the time period 0900 UTC–1500 UTC for each day were considered for the correction. To allow for a comparison of the measurements over the different fields the C_T^2 values were then transformed from the measurement height to an overall aerodynamic reference height of 2 m using Eq. 7. The displacement height was estimated as 2/3 of the actual vegetation height.

4.2 Structure Parameters from the LAS–MWS Data

For the LAS as a single instrument, the measurement of the variances of the logarithm of the signal intensities directly provides C_n^2. C_T^2 can then be derived using Eq. 5, and finally the sensible heat flux, H, is obtained from Eq. 7. However, an estimate of H is needed in Eq. 5 already to obtain *Bo*. To overcome this difficulty, a fixed pre-scribed value of *Bo* may be used. Alternatively, the two equations may be solved iteratively determining *Bo* from $Bo = H/LE$, where LE is the latent heat flux, and parametrizing LE through $LE = 0.9R_{\mathrm{net}} - H$, where R_{net} is the net radiation and the factor 0.9 represents a rough estimate of the effect of the soil heat flux reducing the available energy.

The first results of the combined LAS–MWS measurements to be presented are based on the LASDWD–MWUB system described in Sect. 3.4. From the 500 Hz raw signal intensities the variances of the logarithm of the signal intensities of the LAS and the MWS, respectively $\sigma^2_{\ln(I_{\mathrm{opt}})}$ and $\sigma^2_{\ln(I_{\mathrm{mw}})}$, were calculated as well as the covariance of the log intensities, $\sigma_{\ln(I_{\mathrm{opt}}, I_{\mathrm{mw}})}$. The subscripts *opt* (for optical) and *mw* (for millimetre wave) refer to the wavelengths used by the LAS and the MWS. The relations between the log variances, the log covariance and the structure parameters at the corresponding wavelengths $C^2_{n,\lambda}$ are given by

$$C^2_{n_{\text{opt}}} = 0.893 D^{7/3}_{\text{LAS}} L^{-3} \sigma^2_{\ln(I_{\text{opt}})}, \tag{8a}$$

$$C^2_{n_{\text{mw}}} = 0.248 F^{7/3}_{\text{MWS}} L^{-3} \sigma^2_{\ln(I_{\text{mw}})}, \tag{8b}$$

$$C_{n_{\text{opt}},n_{\text{vmw}}} = 0.576 (D^2_{\text{LAS}} + F^2_{\text{MWS}})^{7/6} L^{-3} \sigma_{\ln(I_{\text{opt}},I_{\text{mw}})}, \tag{8c}$$

where D_{LAS} is the aperture diameter of the LAS, F_{MWS} is the Fresnel zone of the MWS, and L is the pathlength. The constant given in Eq. 8c is only valid for a LAS–MWS set-up with a separation distance between the two systems of 1 m. C^2_T, C^2_q, and C_{Tq} were then determined by combining Eq. 4 written down for the two wavelengths and using the so-called bi-chromatic method described in Lüdi et al. (2005).

4.3 Structure Parameters from the M^{2}AV Data

The temperature structure parameter was determined from the time series of the fast-response temperature measurements aboard of the M^{2}AV using the structure–function method (see Eq. 2 and 3) where V is the true air speed. The structure function of temperature ($D_{TT} = C^2_T r^{-2/3}$) was calculated for the horizontal straight flight legs of 3–5 km length for r varying from the resolution limit ($r < 1$ m) to $r > 1$ km. A double-logarithmic plot of D_{TT} vs. r allows the inertial sub-range to appear as a plateau with a roughly constant value (independence of D_{TT} on r); in our data this typically occurred for 2.5 m $< r <$ 25 m for most of the flights. The mean value of C^2_T over this plateau region (the r range given above) was finally calculated in order to obtain a representative value of C^2_T for each flight leg, and the corresponding statistical error of C^2_T was determined as described in van den Kroonenberg et al. (2012). This method of determining the temperature structure parameter assumes Taylor's hypothesis of frozen turbulence to be fulfilled, implying that the sampling period (e.g. one leg) has to be shorter then the time needed for the turbulence to develop. As the flight time for an individual flight leg was not more then 3–4 min, turbulence was considered frozen and the captured time series could therefore be regarded as a spatial series. Allocation with respect to the ground was obtained by multiplying the measured time series of airborne C^2_T values along each flight leg with the aircraft ground speed.

4.4 Structure Parameters from LES Data

In order to compare and validate the measured structure parameters, comparative simulations with the LES model PALM (Raasch and Schröter 2001) are performed. The structure parameters can be derived from the inertial sub-range of spatial turbulence spectra under homogeneous conditions. Alternatively, temporal spectra and a method based on local similarity, which relates local structure parameters to the dissipation rates of turbulent kinetic energy as well as temperature/humidity, can be used to investigate the variability of the structure parameters along the scintillometer path (e.g. Peltier and Wyngaard 1995; Cheinet and Siebesma 2009). First simulations of a homogeneously heated convective boundary layer with virtual path measurements have been performed.

5 Selected Results

5.1 SLS-20/40 Instrumental Uncertainty

A statistical analysis has been performed on the data collected during the DBSAS intercomparison experiment. The Wageningen SLS-20 (SN221) has been chosen as the reference

Table 4 Results of the statistical inter-comparison of the C_n^2 measurements with five DBSAS SLS-20/40 (reference: Wageningen instrument SN221, Firmware version SLSRun 2.24)

Parameter	System 2	System 3	System 4	System 5
SLS type	SLS-20	SLS-40	SLS-40	SLS-20
Serial number	148	191/192	261	165/166
Firmware version	SLSRun 2.03	SLSRun 2.33	SRun1.05	SLSRun 2.25
Number of data points	272	281	145	136
Correlation coefficient	0.997	0.996	0.984	0.999
Slope of linear regression line	0.94	1.27	1.23	1.05
Mean ($C_n^2(X)/C_n^2$ (WUR221))	0.89	1.23	1.03	0.94
Median ($C_n^2(X)/C_n^2$ (WUR221))	0.91	1.25	1.04	0.95

for this analysis (System 1). Only those 10-min averaging intervals were considered for the comparison for which more then 70 % of the diagnosis data periods were available without error messages from the internal data quality checks. The results are summarized in Table 4.

The number of data points available for the comparison was considerably reduced in the case of systems 4 and 5. While a configuration error resulted in a one-day data loss in the case of system 5, system 4 operates on a completely revised hardware and software basis with an increased internal sampling rate that is higher by more than a factor of 10 when compared to all the other systems. This ensures that the internal statistical data quality tests are more sensitive to any irregularities in the signal characteristics resulting in an increased number of flagged diagnosis data. The correlation coefficient is very high for all systems showing that the data from the different instruments follow the same variations (mainly the pronounced diurnal cycle). The other three scores vary between about 0.89 and 1.28, indicating a deviation of up to about 25 % in the C_n^2 values measured by the different systems. The slope of the regression line suggests that the different instruments do not give the same values; this might be interpreted as a certain percentage of underestimation or overestimation. But the slope is dominated by the high values; possible problems at low values remain hidden. The mean relative value indicates how large, in the mean, the relative deviation is for each sample, but it is not a very robust measure (especially when using relative numbers). That is why we also determined the median relative deviation that gives a more robust indication of the overall relative deviation between the instruments. To assess these relative measures is particularly useful in the case of C_n^2 since it has such a large variation in values. If one would only look at the absolute errors the possible problems at low C_n^2 would completely disappear. While the different measures are consistent for system 2 and system 3, and still show the same tendency for system 4, they provide a different message for system 5 for which apparently the larger values of C_n^2 are overestimated but the lower ones are underestimated (not sufficient to change the slope, but visible in the relative deviations).

It should be noticed that deviations of comparable relative magnitude were found for the inner scale length, l_0. Since errors in C_n^2 and errors in l_0 partially cancel out when calculating the turbulent fluxes, the differences in the sensible heat fluxes are smaller than 5 %. The reasons for these differences are not completely clear. We repeated the inter-comparison exercise in 2010 with three of the five systems over a longer time period (more than one month), with two of the three systems sent to the manufacturer for technical inspection and maintenance before this second experiment. Again, we found deviations of roughly the same magnitude. One possible reason could be the differences in the firmware version. For future

experiments we therefore recommend a harmonization of the firmware used with the different laser scintillometers. In any case, the uncertainty has to be taken into account when interpreting the measurements at the different sites.

5.2 The Temperature Structure Parameter over Different Farmland Surfaces

The structure parameter of temperature C_T^2 close to the surface over five different types of agricultural farmland (barley, colza, grass, maize and triticale) was derived from the SLS-20/40 measurements. Figure 3 (upper panel) shows a time series of the mean daytime value of C_T^2 (calculated over the time period 0900–1500 UTC) for each day of the LITFASS-2009 experiment (June 29–July 24). The data show significant differences (up to an order of magnitude or even higher) between the different types of farmland. This is an important result with respect to the overall goal of the LITFASS-2009 experiment—if there was no significant contrast at ground level we would not have to assess C_T^2 variability along a LAS path over heterogeneous terrain. The differences can be explained by the status of the vegetation. This is further illustrated by the mean daytime values of the Bowen ratio determined from the eddy-covariance measurements at the micrometeorological sites (Fig. 3, lower panel). Barley and triticale were already senescent and very dry during the experiment and hence the observed C_T^2 as well as *Bo* are high. There are no data for barley after July 14, 2009, when the harvest took place. The maize was in a phase of rapid vegetation development and actively transpiring (during LITFASS-2009 the plants grew from a height of about 0.3 m to more than 2 m). Consequently the observed C_T^2 is relatively low, and the daytime mean values decrease during the experiment (as a tribute to the increasing portion of available energy going into the latent heat flux also reflected in an overall decreasing mean *Bo*) while there is no obvious trend at the other sites. The inter-diurnal variability of daytime C_T^2 values reaches up to about half an order of magnitude. It is basically a tribute to the cloud cover and radiation conditions, where relatively small values of the daily sum of global radiation were measured on July 02, 06, 14 and 18, in particular.

It is important to note that the differences between the different plants during daytime usually exceed the instrumental uncertainty found from the laser scintillometer inter-comparison (Sect. 5.1). With the assessment of the differences we are even on the safe side: the Wageningen SLS-20 (SN221), which served as a reference for the inter-comparison, was operated over triticale during the main field phase. System 2 operated over barley, a correction of the too low values (see Table 4) would thus further increase the difference between barley and triticale, and the opposite holds for the other three systems.

5.3 The Variability of C_T^2 Along the LAS Path

The spatial series of C_T^2 along a single M^2AV flight leg was calculated using a moving window over which the structure function $D_{TT}(r)$ was computed. This window, which had a width of 15 s (corresponding to a length of 330 m), was applied to each data point i of the temperature time series with i as the centre point. By moving this window over the whole data series representing one flight leg the semi-local temperature structure parameter $C_T^2(i)$ was calculated. This resulted in C_T^2 values at a time resolution of 0.01 s (corresponding to a spatial distance of about 0.2 m). A more detailed description of this methodology is given in van den Kroonenberg et al. (2012), including a justification for the choice of the window width.

For the flights made during midday the variability along the path is considerable (Fig. 4). At the lower level, C_T^2 values vary by a factor of 5–10 along the flight leg, and at the upper

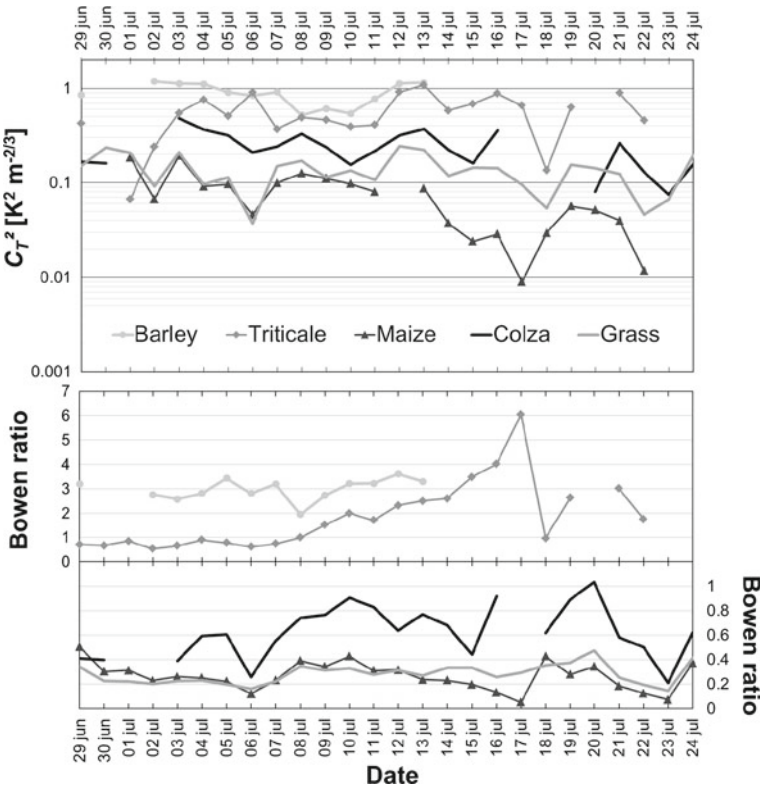

Fig. 3 Time series of the mean daytime values of normalized temperature structure parameter (see Sect. 4.1), C_T^2 (*upper panel*), and of the Bowen ratio, *Bo* (*lower panel*), at the different farmland sites over the period of the experiment

level the variability reaches a factor of 2–5, which is still substantial. This variability can, to a large part, be attributed to convective updrafts and downdrafts. This is illustrated by the dashed lines in Fig. 4 that show the variability of vertical wind speed, w, as measured by the M^{2}AV aircraft along the north-south flight legs at the two levels. The original w time series were filtered by a 15-s moving average in order to be consistent with the determination of C_T^2. The mean vertical wind speed averaged over the leg was -0.034 and $-0.168\,\mathrm{m\,s^{-1}}$ at 58 and 84 m, respectively. It can be clearly seen that the position of the relative maxima of C_T^2 and w mostly coincide.

Moreover, it becomes obvious, e.g. from the comparison of the C_T^2 spatial series at the lower flight level, that the position of the maxima and minima varies within a few minutes. It is thus impossible to directly relate spatial structures from a single flight leg to certain characteristics of the underlying surface. We remark that the maize field with low near-surface values of C_T^2 was situated below the southern part of the flight legs (see Fig. 1). We conclude that, based on the data from just a single flight, it is not clear if certain structures in the spatial pattern of C_T^2 can be directly related to distinct surface structures. More flights at the same level and under undisturbed quasi-stationary weather conditions (and possibly even simultaneous flights with several aircraft at different heights) are needed to study these effects in more detail.

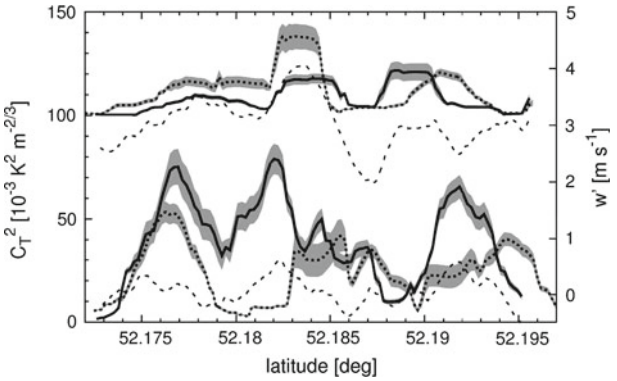

Fig. 4 Spatial variability of C_T^2 values along the LAS path for the "scintillometer profile" flights on July 13, 2009, between 1226 UTC and 1241 UTC. For better visibility, the spatial series measured at 84 m are displayed with an offset of 100×10^{-3} K^2 m$^{-2/3}$ to the spatial series below, which corresponds to the measurements at 58 m. The *solid lines* represent the south-north flights, the *dotted lines* the north-south flights, respectively, *grey shading marks* the statistical uncertainty determined according to van den Kroonenberg et al. (2012). *Dashed lines mark* the vertical velocity for the south-north legs, the upper flight level displayed with an offset of 3 m s^{-1}

5.4 Comparison of C_T^2 Data from LAS and M^{2}AV Measurements

The daytime evolution of C_T^2 as derived from the DBSAS, LAS and aircraft data for July 13, 2009 is depicted in Fig. 5. From the surface-layer measurements, only the barley and grass data are shown representing two farmland types with a typical high and low value, respectively (see Sect. 5.2). Data are plotted only if more than 70 % of the diagnosis data intervals during a 10-min sampling period were not flagged as erroneous. For the grassland data, the thick line compared to the thin line illustrates the effect of the *Bo* correction (where the thick line marks the corrected data). For barley this correction is irrelevant due to the high *Bo* values (see Eq. 5 and Fig. 3).

The diurnal variation of C_T^2 is basically consistent between the different measurement systems. Pronounced minima occur after sunrise (around 0500 UTC) and around sunset (1900 UTC), and their occurrence is slightly delayed at the LAS levels when compared to the surface-layer measurements. The afternoon decrease of C_T^2 is generally in good agreement between the LAS and aircraft data. During the daytime, C_T^2 typically decreases with height (under free convective conditions: $C_T^2 \sim z^{-4/3}$). As a result, the LAS and aircraft observed values are a factor 10–100 smaller than the ground observations. Furthermore, the order-of-magnitude values are comparable for the LAS and aircraft measurements with values around 10^{-2} K^2 m$^{-2/3}$ during the early afternoon and much smaller values ($1–5 \times 10^{-4}$ K^2 m$^{-2/3}$) in the evening. However, in-situ aircraft measurements at a height of about 54 m provided systematically larger values of C_T^2 than those derived from the LAS at 43 m, which contradicts the theory and is subject to further investigation.

5.5 Vertical Profiles of C_T^2

Vertical profiles of C_T^2 on July 13, 2009, at 1100, 1400 and 1700 UTC are shown in Fig. 6. The scintillometer data have been averaged over one hour, while the aircraft data are an average over the different legs performed within the time period indicated. The surface-layer data are an average of the measurements over barley and triticale, the two stations in the centre of

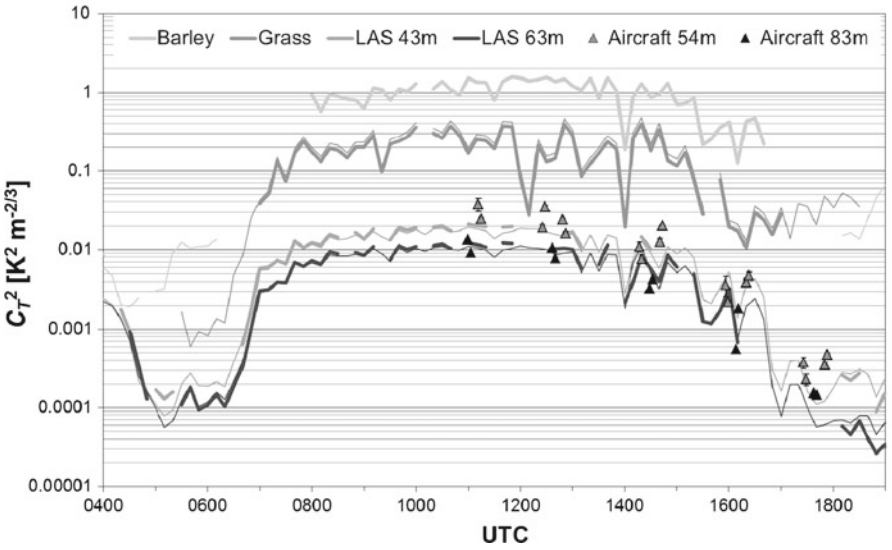

Fig. 5 Daytime evolution of C_T^2 on July 13, 2009: LAS: path-averaged (*bold line* using *Bo* determined by iteration—see Sect. 4.2, *thin line* using a fixed value of $Bo = 1$). Aircraft: leg-averaged (see Sect. 4.3). Barley and grass: SLS field measurements

the LAS path that are assumed to be most closely related to the LAS signal taking into account the systems path-weighting function. At a later stage of our analysis, footprint calculations are performed in order to allow for an adequate averaging of the contributions from all the five surface stations. Around noon and in the early afternoon (1100 UTC–1400 UTC) the decrease of C_T^2 between the surface layer and the lower LAS level is almost proportional to $z^{-4/3}$ as explained by free-convective theory. In the evening, around 1700 UTC, the decrease with height is greater: free-convective theory is no longer applicable during the evening transition period. In contrast to this, the aircraft data do not fit the $z^{-4/3}$ law. Possible explanations are the different spatial weighting of the LAS and the aircraft and different land-use patterns in the footprint area, especially for the flights at 83 m, but further detailed analysis of the flight data is necessary to prove this hypotheses. It should also be mentioned that both methods sample a different part of the turbulent spectrum. If there is any discontinuity in the inertial sub-range, this would lead to a discrepancy. To study this we suggest to use small, fast-response thermocouples in the mast to sample the inertial sub-range down to well below the 0.15-m scale.

5.6 The Influence of Tower Vibrations on the Scintillometer Measurements

In order to study the potential influence of tower vibrations on the LAS–MWS measurements, both of these systems were fitted with accelerometers to monitor their movement and vibrations (see Sect. 3.3). As an example of the results, Fig. 7 shows spectra of the scintillometer signals and of the accelerations for one 30-min interval during the experiment. The mean wind speed at 40 m during this period was 6.6 m s^{-1}, and theoretical spectra according to Clifford (1971) are shown for comparison. It can be seen that the LAS spectra compare well with the theoretical spectra, whereas the MWS spectra show some bumps that are likely to be related to tower vibrations. For the MWUB (see Sect. 3.3 for the explanation of this abbreviation,

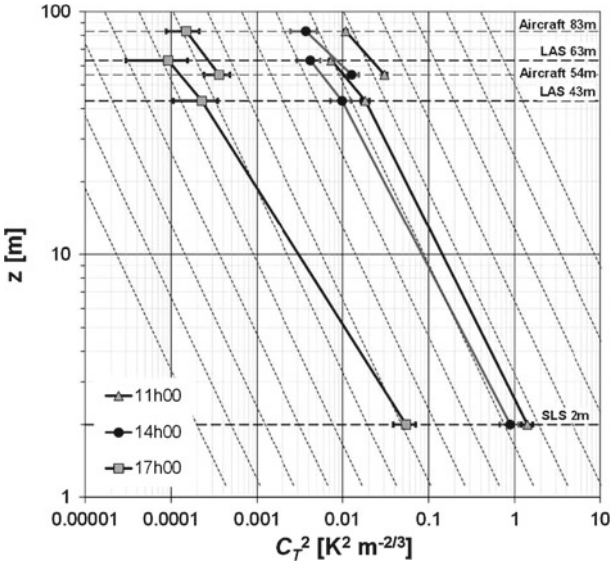

Fig. 6 Vertical profiles of C_T^2 on July 13, 2009, at 1100, 1400 and 1700 UTC, averaged over 1 h for the scintillometers and over the different legs for the aircraft. The *horizontal dashed lines* show the measurement levels and the *diagonal dashed lines* show the expected profile slope for the free convective limit ($C_T^2 \sim z^{-4/3}$)

as well as for MWRAL) it can be seen that the bumps in the spectrum are visible in the log-log representation of the spectrum (top right sub-figure), but the semi-log representation of the spectrum, which is proportional to the total variance of the signal, reveals that these bumps have little effect on $\sigma^2_{ln(I)}$ (below top right sub-figure). In addition, the measurement curve follows the shape of the theoretical spectrum adequately. The MWRAL performs much worse on both these aspects, i.e., a bump can be seen that contributes significantly to $\sigma^2_{ln(I)}$ (below top left sub-figure) and it deviates from the theoretical shape. It is not exactly clear to what effect the ill-performance of the MWRAL can be attributed, but it seems to be related to instrumental issues and not to the difference in set-up with respect to the MWUB. The accelerometer spectra show tower movements on many temporal scales, some of which coincide with the bumps in the MWS spectra but most do not seem to affect the MWS nor LAS spectra. Even accelerometer spectra filtered to frequencies that are most likely associated with tower vibrations (lowest two sub-figures in Fig. 7) do not show a clear relation with the bumps in the scintillometer spectra. We conclude that our initial idea that any tower vibration should be visible in the scintillometer spectrum is too simple. Further investigation is needed as to why certain types or frequencies of vibrations do show up and others do not. Figure 7 shows only one 30-min interval to illustrate this point. Inspection of the 30-min spectra for the whole experiment shows that the conclusion we draw here is a general one.

Figure 8 shows the relation between the standard deviation of the accelerometer data (which is a measure for the intensity of the tower vibrations) and wind speed. It is clear that the 99-m tall Falkenberg tower exhibits much more movement than the smaller and structurally more rigid Lindenberg tower. For the Falkenberg tower, the standard deviations of the accelerometer output are about one order of magnitude higher than for the MOL-RAO tower, moreover a clear dependence on wind speed and wind direction becomes obvious. Especially when the wind direction is from the south (LAS–MWS systems are installed on the north side of the Falkenberg tower) and not fluctuating much, i.e. having a small standard

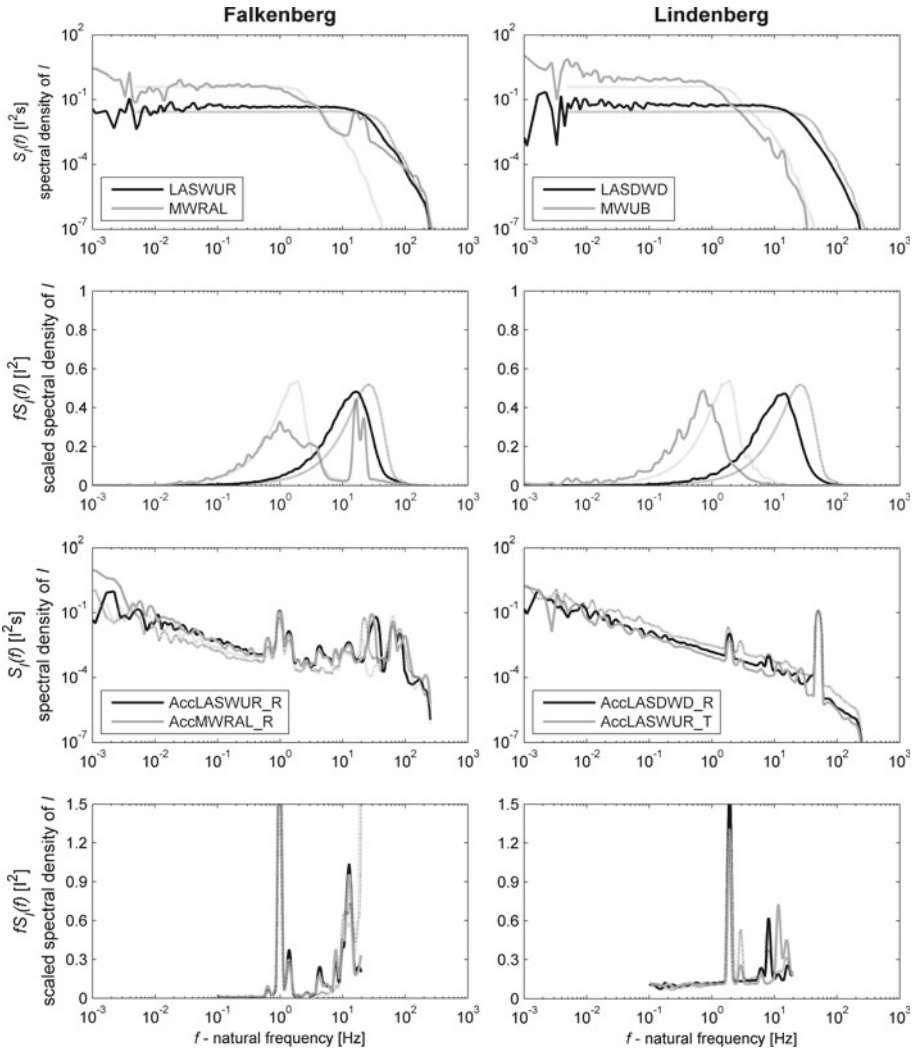

Fig. 7 Spectra of the LAS–MWS systems (*top four sub-figures*) and their corresponding accelerometers (*lower four sub-figures*) for the Falkenberg tower (*left*) and Lindenberg tower (*right*) on July 13, 0100–0130 UTC. The LAS–MWS spectra in *solid lines* are measured spectra, in *dotted lines* the theoretical spectra are given. The accelerometer spectra in *solid lines* refer to horizontal movement, in *dotted lines* to vertical movement. The *first* and *third row* show a log–log representation of the power spectra to reveal the slope of the spectra, whereas the *second* and *fourth row* show the semi-log representation of the frequency times the spectrum to show the relative contribution of each frequency to the variance

deviation in wind direction, the tower vibrations are strongest for relatively low wind speeds of 6 and 8 m s^{-1}. These conditions seem to define the eigenfrequency of the tower.

5.7 Combined LAS–MWS Measurements

As a last example of the results obtained, we present in Fig. 9 the time series of C_n^2 for optical and microwave wavelengths ($C_{n,\mathrm{opt}}^2$ and $C_{n,mw}^2$) and their cross structure parameter

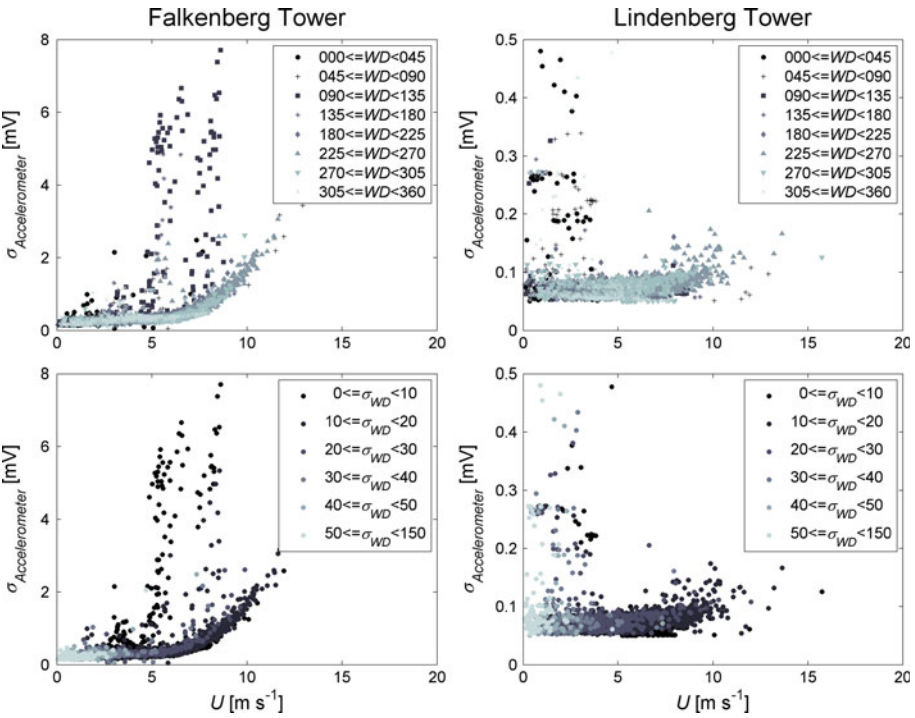

Fig. 8 30-min standard deviation of one of the accelerometers registering the orthogonal movement of the LAS units at the GM Falkenberg (*left*) and MOL-RAO (*right*) towers versus wind speed. Data points are colour-coded according to the mean wind direction (*top figures*) and standard deviation in wind direction (*bottom figures*). In the legend, *WD* is the wind direction, and σ_{WD} is twice its standard deviation

($C_{n,\mathrm{opt}-n,\mathrm{mw}}$) as derived from the LASDWD–MWUB system for July, 12–13, 2009. From these, we determined C_T^2, C_q^2 and C_{Tq} following the bi-chromatic technique by Lüdi et al. (2005), see Sect. 4.2. These "meteorological" structure parameters are depicted in Fig. 10.

The weather during the two days was characterized by a continuously changing cloud cover that explains the short-term variability of all structure parameters superimposed on their daily cycle. In the early morning of 12 July fog occurred and in the early evening of that same day it rained. This explains the loss of data for these periods.

Figure 9 shows that $C_{n,\mathrm{mw}}^2$ is typically one order of magnitude larger that $C_{n,\mathrm{opt}}^2$, and the cross structure parameter $C_{n,\mathrm{opt}-n,\mathrm{mw}}$ is negative during the day and positive during nighttime. This cross structure parameter in itself is not so interesting, for our application it is merely a necessary parameter to solve C_T^2 and C_q^2 using the bi-chromatic technique. C_T^2 and C_q^2 are used to calculate the sensible and latent heat flux. As a bonus, the bi-chromatic technique also gives C_{Tq}, which is related to r_{Tq} (Eq. 6) and thus provides the sign of the sensible heat flux.

Figures 9 and 10 together corroborate the points made on the C_n^2 to C_T^2, C_q^2 and C_{Tq} relation following Eq. 4, namely that C_T^2 is dominant in $C_{n,\mathrm{opt}}^2$ whereas C_q^2 is dominant in $C_{n,\mathrm{mw}}^2$, i.e. the shapes of these time series are very similar. C_{Tq} has the reverse sign of $C_{n,\mathrm{opt}-n,\mathrm{mw}}$, i.e. positive under unstable conditions and negative under stable conditions. It seems that the light rainfall in the evening of July 12 boosted the evapotranspiration in the LASDWD–MWUB footprint, resulting in a higher $C_{n,\mathrm{mw}}^2$ and C_q^2 than the previous day.

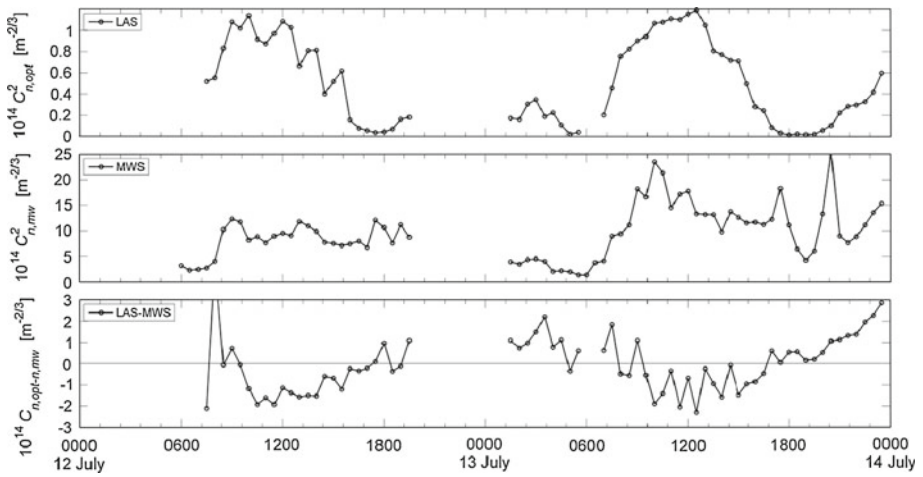

Fig. 9 Time series of $C^2_{n,\mathrm{opt}}$, $C^2_{n,\mathrm{mw}}$, and $C^2_{n,\mathrm{opt-mw}}$ for the LASDWD–MWUB system on July 12–13, 2009

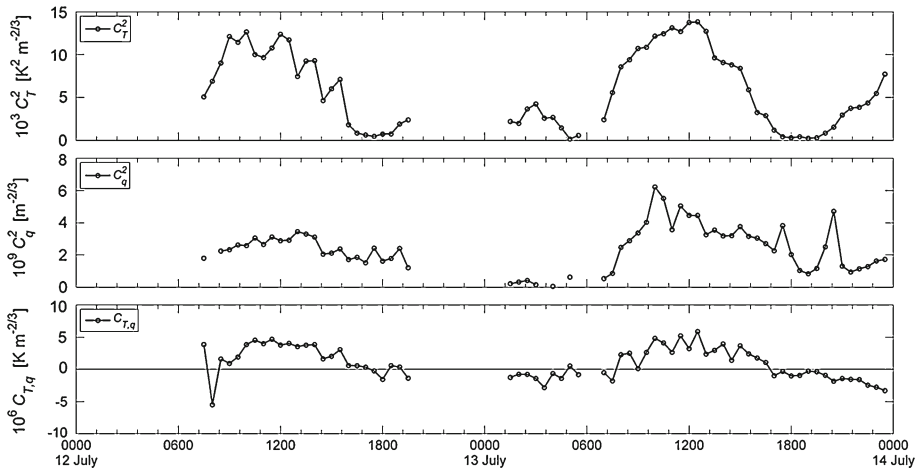

Fig. 10 Time series of C^2_T, C^2_q, and C_{Tq} for the LASDWD–MWUB system on July 12–13, 2009

6 Summary, Conclusions and Outlook

The LITFASS-2009 experiment was designed to study certain aspects of the use of scintillometers to derive area-averaged heat fluxes over a heterogeneous land surface. A special focus was set on the validation of the temperature structure parameters derived from the scintillometer data by independent airborne measurements performed along the scintillometer path.

Two LAS–MWS systems were operated over a path length of 4.9 km at effective heights of 43 and 63 m above ground level, respectively. Five micrometeorological stations equipped with eddy-covariance instrumentation for turbulent flux measurements were set up over five different types of agricultural farmland in the footprint area of the LAS–MWS path. At each of these stations a laser scintillometer was operated to derive the structure parameters near

to the ground. 16 flights with the unmanned aircraft M^2AV were performed on six days to measure the temperature fine structure of the lower atmosphere along the LAS–MWS path. Temperature structure parameters were derived from the laser scintillometer, LAS and aircraft measurements.

Before being installed at the farmland sites, the five laser scintillometers were operated side by side at the Falkenberg boundary-layer field site over a period of three days. Intercomparison of the refractive-index structure parameters measured with the five systems revealed relative deviations of up to 25–30 %. This could be considered as substantial. However one has to keep in mind the large variability of C_n^2 over two to three orders of magnitude during the diurnal cycle. It should be remarked again that the differences in the refractive-index structure parameter are largely compensated by oppositely directed differences in the inner-scale length such that the sensible heat fluxes derived from the systems typically agree within 5 %.

The height-normalized temperature structure parameter close to the ground significantly differed between the five types of farmland depending on the status of vegetation development. High values over senescent cereals (barley, triticale) contrasted with low values over the growing maize and grass. The differences were typically larger than the deviations found in the scintillometer inter-comparison experiment.

With the LAS–MWS systems we found clear indications of tower vibrations in the spectra of the intensity fluctuations for higher wind speeds (as have been reported earlier for the Lindenberg–Falkenberg path by, e.g., Meijninger et al. 2006). These particularly affect the MWS measurements, whereas for the LAS their contribution to the overall variance (and hence to the derived structure parameters) can be mostly neglected. For the first time we were able to study these vibrations with the help of accelerometers attached to the LAS–MWS transmitter and receiver units. However, the accelerometers showed many more peaks in the spectra than did the scintillometers, such that direct use of the accelerometer data to correct the LAS–MWS spectra appears to be not possible, and more research is needed to understand the relationship between the accelerometer and scintillometer signals.

One of our primary goals was the independent validation of the temperature structure parameter derived from LAS data by the use of aircraft measurements. C_T^2 values derived from the aircraft measurements were on the same order of magnitude as the LAS data. The variation during daytime between large values around noon and small values around sunset and sunrise could be well reproduced from the aircraft data. However, the measurements at the lowest flight level showed a tendency towards a systematic overestimation when compared with the LAS-based values. Consequently, the decrease with height was greater than predicted by free-convective scaling. Further analysis must show to what extent this has to be attributed to the different spatial, temporal and statistical representativity of the aircraft and LAS measurements.

A detailed analysis of the variation of the temperature structure parameter along the flight legs revealed substantial spatial variability that could be basically attributed to single convective plumes. A separation of the effects of the statistical nature of turbulence from those of the heterogeneity of the underlying surface on the spatial variability of the structure parameters along a LAS–MWS path appears to be a crucial task in order to understand the scintillometer signals. Here we have to take into account the different sampling characteristics of the different systems. The (spatial or temporal) (inherent turbulent) variability of the structure parameters depends on the scale at which averaging takes place: the variability decreases with the increase of the averaging length (e.g., Cheinet and Siebesma 2009). As we are interested in the variability of the structure parameter due to surface heterogeneity, we wish to remove the variability due to turbulence. The averaging scale needed to suppress the turbulent variability

to an admissible level will set the upper limit of detectable spatial structures linked to the surface heterogeneity. Concerning our flight strategy, longer flight legs or several repeated flights along the shorter leg might be necessary to provide statistics over a larger number of plumes and quieter zones in between, but also to assign variations to the underlying surface. To further substantiate these initial results with respect to the diurnal cycle, a second small flight campaign with the M^2AV has been performed on two clear-sky days in July 2010. First results from this second experiment can be found in van den Kroonenberg et al. (2012). Moreover, fast response in-situ temperature measurements at different levels on the 99-m tower should provide an estimate of the turbulent variability of the structure parameters over different integration times, since heterogeneity effects would not influence the single-point measurements.

Referring to the open issues in the area of scintillometry discussed in Sect. 2 it becomes obvious that our initial results presented in Sect. 5 do not address all these questions. They can rather be seen as a starting point of a more in-depth analysis of the data that will provide further results on which we intend to report at a later date.

Concerning the experimental strategy, we conclude that our set-up appeared to be suited to study the behaviour of C_T^2 in the lower boundary layer over a heterogeneous landscape. With the M^2AV aircraft we were able to fly along a LAS path at low heights and with small variations in flight altitude (1–2 m). C_T^2 values with reasonable statistical uncertainty could be derived using the structure function method. We therefore conclude that M^2AV measurements are a suitable technique to derive C_T^2 at the 2–5 km scale along the path of a LAS.

Based on the experiences from the LITFASS-2009 experiment and from the 2010 flight campaign, another scintillometry experiment would be a logical follow-up effort. Such a campaign should extend the experimental approach to humidity structures and to larger scales of a more heterogeneous surface covered by high vegetation (forest), low vegetation (farmland) and open water. In more detail, such an experiment should have the following basic goals:

- to derive the complete set of structure parameters (C_T^2, C_q^2, and C_{Tq}) from scintillometer measurements with a coupled LAS–MWS system over the Lindenberg–Falkenberg path and from flight measurements along this path for comparison and assessment of the scintillometer principle,
- to study the behaviour of structure parameters (horizontal variability, vertical profiles, possible existence of a blending height) over more complex terrain by performing LAS and airborne measurements along different scintillometer paths representing heterogeneous farmland (as in LITFASS-2009), forest, open water, and mixed terrain also including LES for the larger area comprising the different types of land use,
- to study the similarity between the turbulent temperature and humidity fields and to assess the consequences of a possible dissimilarity on the temperature-humidity correlation and on the similarity functions applied to derive the turbulent fluxes from the scintillation measurements.

Acknowledgements The LITFASS-2009 experiment was performed as part of the research project "Turbulent structure parameters over heterogeneous terrain—implications for the interpretation of scintillometer data". This project is funded by the German Science Foundation (Deutsche Forschungsgemeinschaft, DFG) through grants BA1988/9-1, BE2044/3-1, RA617/20-1, and by the Dutch Science Foundation (Nederlandse Organisatie voor Wetenschappelijk Onderzoek, NWO) through grant DN76-274. The DBSAS operated in the maize field has been provided by the Meteorological Institute of the University of Leipzig in co-operation with the Institute for Tropospheric Research Leipzig, thanks go to A. Raabe and T. Conrath. The MWRAL system was provided by the Centre for Ecology and Hydrology Wallingford, UK, the authors are thankful to J. Evans and H. Ward. Significant support in performing the measurements and preparing the data came from the MOL-RAO staff members P. Dereszynski, C. Heret, G. Hollaz, J. Janiak, K. Jantze, S. Niesche, S.H.

Richter, U. Rummel, M. Schwebe and P. Ulrych. M. Böhm and C. Behrens did an excellent job as safety pilots of the M^2AV aircraft. Finally we would like to thank the two anonymous reviewers who gave valuable comments on the initial version of the paper.

References

Allen RG, Pereira LS, Howell TA, Jensen ME (2011) Evapotranspiration information reporting: I. Factors governing measurement accuracy. Agric Water Manag 98:899–920

Andreas EL (1989) The refractive-index structure parameter, C_n^2, for a year over the Frozen Beaufort Sea. Radio Sci 24:667–679

Asanuma J, Iemoto K (2007) Measurements of regional sensible heat flux over mongolian grassland using large aperture scintillometer. J Hydrol 333:58–67

Bange J, Beyrich F, Engelbart DAM (2002) Airborne measurements of turbulent fluxes during litfass-98: comparison with ground measurements and remote sensing in a case study. Theor Appl Climatol 73:35–51

Bange J, Zittel P, Spiess T, Uhlenbrock J, Beyrich F (2006a) A new method for the determination of area-averaged turbulent surface fluxes from low-level flights using inverse models. Boundary-Layer Meteorol 119:527–561

Bange J, Spiess T, Herold M, Beyrich F, Hennemuth B (2006b) Turbulent fluxes from helipod flights above quasi-homogeneous patches within the LITFASS area. Boundary-Layer Meteorol 121:127–151

Beyrich F, Mengelkamp HT (2006) Evaporation over a heterogeneous land surface: EVA_GRIPS and the LITFASS-2003 experiment—an overview. Boundary-Layer Meteorol 121:5–32

Beyrich F, De Bruin HAR, Meijninger WML, Schipper JW, Lohse H (2002a) Results from one-year continuous operation of a large aperture scintillometer over a heterogeneous land surface. Boundary-Layer Meteorol 105:85–97

Beyrich F, Herzog HJ, Neisser J (2002b) The LITFASS project of DWD and the LITFASS-98 experiment: the project strategy and the experimental setup. Theor Appl Climatol 73:3–18

Beyrich F, Kouznetsov RD, Leps JP, Lüdi A, Meijninger WML, Weisensee U (2005) Structure parameters of temperature and humidity from simultaneous eddy-covariance and scintillometer measurements. Meteorol Z 14:641–649

Beyrich F, Leps JP, Mauder M, Bange J, Foken T, Huneke S, Lohse H, Lüdi A, Meijninger WML, Mironov D, Weisensee U, Zittel P (2006) Area-averaged surface fluxes over the LITFASS region based on eddy-covariance measurements. Boundary-Layer Meteorol 121:33–65

Businger JA, Wyngaard JC, Izumi Y, Bradley EF (1971) Flux–profile relationships in the atmospheric surface layer. J Atmos Sci 28:181–189

Cammalleri C, Agnese C, Ciraolo G, Minacapilli M, Provenzano G, Rallo G (2010) Actual evapotranspiration assessment by means of a coupled energy/hydrologic balance model: validation over an olive grove by means of scintillometry and measurements of soil water content. J Hydrol 392:70–82

Chandrapala L, Wimalasuriya M (2003) Satellite Measurements supplemented with meteorological data to operationally estimate evaporation in Sri Lanka. Agric Water Manag 58:89–107

Cheinet S, Siebesma AP (2009) Variability of local structure parameters in the convective boundary layer. J Atmos Sci 66:1002–1017

Clifford SF (1971) Temporal-frequency spectra for a spherical wave propagating through atmospheric turbulence. J Opt Soc Am 61:1285–1292

De Bruin HAR, Kohsiek W, Vanden Hurk BJJM (1993) A verification of some methods to determine the fluxes of momentum, sensible heat, and water-vapour using standard-deviation and structure parameter of scalar meteorological quantities. Boundary-Layer Meteorol 63:231–257

De Bruin HAR, Vanden Hurk B, Kohsiek W (1995) The scintillation method tested over a dry vineyard area. Boundary-Layer Meteorol 76:25–40

De Bruin HAR, VanDen Hurk B, Kroon LJM (1999) On the temperature-humidity correlation and similarity. Boundary-Layer Meteorol 93:453–468

De Bruin HAR, Meijninger WML, Smedman ASM, Magnusson M (2002) Displaced-beam small aperture scintillometer test. Part I: the wintex data-set. Boundary-Layer Meteorol 105:129–148

Ek MB, Holtslag AAM (2005) Evaluation of a land-surface scheme at Cabauw. Theor Appl Climatol 80: 213–227

Evans JG (2009) Long-path scintillomtery over complex terrain to measure area-averaged sensible and latent heat fluxes. PhD Thesis, The University of Reading, 176 pp

Ezzahar J, Chehbouni G, Hoedjes JCB, Chehbouni A (2007a) On the application of scintillometry over heterogeneous grids. J Hydrol 334:493–501

Ezzahar J, Chehbouni G, Hoedjes JCB, Er-Raki S, Chehbouni A, Boulet G, Bonnefond JM, De Bruin HAR (2007b) The use of the scintillation technique for monitoring seasonal water consumption of olive orchards in a semi-arid region. Agric Water Manag 89:173–184

Ezzahar J, Chehbouni A, Hoedjes J, Ramier D, Boulain N, Boubkraoui S, Cappelaere B, Descroix L, Mougenot B, Timouk F (2009) Combining scintillometer measurements and an aggregation scheme to estimate area-averaged latent heat flux during the AMMA experiment. J Hydrol 375:217–226

Foken T, Kretschmer D (1990) Stability dependence of the temperature structure parameter. Boundary-Layer Meteorol 53:185–189

Green AE, Green SR, Astill MS, Caspari HW (2000) Estimating latent heat flux from a vineyard using scintillometry. Terr Atmos Ocean Sci 11:525–542

Green AE, Astill MS, McAneney KJ, Nieveen JP (2001) Path-averaged surface fluxes determined from infrared and microwave scintillometers. Agric For Meteorol 109:233–247

Gryning SE, Halldin S, Lindroth A (2002) Area averaging of land surface-atmosphere fluxes in NOPEX: challenges, results and perspectives. Boreal Environ Res 7:379–387

Hartogensis OK, De Bruin HAR (2005) Monin–Obukhov similarity functions of the structure parameter of temperature and turbulent kinetic energy dissipation rate in the stable boundary layer. Boundary-Layer Meteorol 116:253–276

Hartogensis OK, De Bruin HAR, Vande Wiel BJH (2002) Displaced-beam small aperture scintillometer test. Part II: CASES-99 stable boundary-layer experiment. Boundary-Layer Meteorol 105:149–176

Hill RJ (1997) Algorithms for obtaining atmospheric surface-layer fluxes from scintillation measurements. J Atmos Ocean Technol 14:456–467

Hill RJ, Clifford SF, Lawrence RS (1980) Refractive-index and absorption fluctuations in the infrared caused by temperature, humidity, and pressure-fluctuations. J Opt Soc Am 70:1192–1205

Hill RJ, Bohlander RA, Clifford SF, McMillan RW, Priestley JT, Schoenfeld WP (1988) Turbulence-induced millimeter-wave scintillation compared with micrometeorological measurements. IEEE Trans Geosci Remote Sens 26:330–342

Hoedjes JCB, Zuurbier RM, Watts CJ (2002) Large aperture scintillometer used over a homogeneous irrigated area, partly affected by regional advection. Boundary-Layer Meteorol 105:99–117

Hoedjes JCB, Chehbouni A, Ezzahar J, Escadafal R, De Bruin HAR (2007) Comparison of large aperture scintillometer and eddy covariance measurements: can thermal infrared data be used to capture footprint-induced differences?. J Hydrometeorol 8:144–159

Holtslag AAM, Duynkerke PG (eds) (1998) Clear and cloudy boundary layers. Koninklijke Nederlandse Akademie van Wetenschappen, Amsterdam, 372 pp

Kleissl J, Gomez J, Hong SH, Hendrickx JMH, Rahn T, Defoor WL (2008) Large aperture scintillometer intercomparison study. Boundary-Layer Meteorol 128:133–150

Kleissl J, Hong SH, Hendrickx JMH (2009a) New Mexico scintillometer network: supporting remote sensing and hydrologic and meteorological models. Bull Am Meteorol Soc 90:207–218

Kleissl J, Watts CJ, Rodriguez JC, Naif S, Vivoni ER (2009b) Scintillometer intercomparison study continued. Boundary-Layer Meteorol 130:437–443

Kohsiek W (1982) Measuring C_T^2, C_Q^2, and C_{TQ} in the unstable surface-layer, and relations to the vertical fluxes of heat and moisture. Boundary-Layer Meteorol 24:89–107

Kohsiek W, Herben M (1983) Evaporation derived from optical and radiowave scintillation. Appl Opt 22:2566–2570

Kohsiek W, Meijninger WML, Moene AF, Heusinkveld BG, Hartogensis OK, Hillen W, De Bruin HAR (2002) An extra-large aperture scintillometer for long range applications. Boundary-Layer Meteorol 105:119–127

Kohsiek W, Meijninger WML, De Bruin HAR, Beyrich F (2006) Saturation of the large aperture scintillometer. Boundary-Layer Meteorol 121:111–126

Lagouarde JP, Jacob J, Gu XF, Olioso A, Bonnefond JM, Kerr Y, McAneney KJ, Irvine M (2002) Spatialization of sensible heat flux over a heterogeneous landscape. Agronomie 22:627–633

Lagouarde JP, Irvine M, Bonnefond JM, Grimmond CSB, Long N, Oke TR, Salmond JA, Offerle B (2006) Monitoring the sensible heat flux over urban areas using large aperture scintillometry: case study of Marseille city during the escompte experiment. Boundary-Layer Meteorol 118:449–476

Lee X, Massman W, Law B (eds) (2004) Handbook of micrometeorology. Kluwer, Dordrecht/Boston/London p 250

LeMone MA, Chen F, Alfieri JG, Tewari M, Geerts B, Miao Q, Grossman RL, Coulter RL (2007) Influence of land cover and soil moisture on the horizontal distribution of sensible and latent heat fluxes in Southeast Kansas During IHOP-2002 and CASES-97. J Hydrometeorol 8:68–87

Lüdi A, Beyrich F, Mätzler C (2005) Determination of the turbulent temperature–humidity correlation from scintillometric measurements. Boundary-Layer Meteorol 117:525–550

Mahrt L, Vickers D, Sun JL, McCaughey JH (2001) Calculation of area-averaged fluxes: application to BOREAS. J Appl Meteorol 40:915–920

Martin S, Bange J, Beyrich F (2011) Meteorological profiling of the lower troposphere using the research UAV "M^2AV Carolo". Atmos Meas Tech 4:705–716

McAneney KJ, Green AE, Astill MS (1995) Large-aperture scintillometry—the homogeneous case. Agric For Meteorol 76:149–162

Meijninger WML, de Bruin HAR (2000) The sensible heat fluxes over irrigated areas in Western Turkey determined with a large aperture scintillometer. J Hydrol 229:42–49

Meijninger WML, Moene A, Hartogensis OK, De Bruin HAR, Heusinkveld BG (2000) Large-Aperture Scintillometer: User Manual and Technical Information. Wageningen University, Wageningen, The Netherlands, 63 pp

Meijninger WML, Hartogensis OK, Kohsiek W, Hoedjes JCB, Zuurbier RM, De Bruin HAR (2002a) Determination of area-averaged sensible heat fluxes with a large aperture scintillometer over a heterogeneous surface—Flevoland field experiment. Boundary-Layer Meteorol 105:37–62

Meijninger WML, Green AE, Hartogensis OK, Kohsiek W, Hoedjes JCB, Zuurbier RM, De Bruin HAR (2002b) Determination of area-averaged water vapour fluxes with large aperture and radio wave scintillometers over a heterogeneous surface—Flevoland field experiment. Boundary-Layer Meteorol 105:63–83

Meijninger WML, Beyrich F, Lüdi A, Kohsiek W, De Bruin HAR (2006) Scintillometer-based turbulent fluxes of sensible and latent heat over a heterogeneous land surface—a contribution to LITFASS-2003. Boundary-Layer Meteorol 121:89–110

Moene AF (2003) Effects of water vapour on the structure parameter of the refractive index for near-infrared radiation. Boundary-Layer Meteorol 107:635–653

Moene AF, Meijninger WML, Hartogensis OK, Heusinkveld BG, De Bruin HAR (2005) The Effect of Finite Accuracy in the Manufacturing of Large-Aperture Scintillometers Wageningen University, Wageningen, The Netherlands, 20 pp

Moene AF, Meijninger WML, Kohsiek W, Gioli B, Miglietta F, Bosveld F (2006a) Validation of fluxes of an extra large aperture scintillometer at Cabauw using sky arrow aircraft flux measurements. In: Proceedings of 17th symposium on boundary layers and turbulence. American Meteorological Society, San Diego, CA, 22–25 May 2006

Moene AF, Schüttemeyer D, Hartogensis OK (2006b) Scalar similarity functions: the influence of surface heterogeneity and entrainment. In: Proceedings of 17th symposium on boundary layers and turbulence. American Meteorological Society, San Diego, CA, 22–25 May 2006

Moene AF, Michels BI, Holtslag AAM (2006c) Scaling variances of scalars in a convective boundary layer under different entrainment regimes. Boundary-Layer Meteorol 120:257–274

Neisser J, Adam W, Beyrich F, Leiterer U, Steinhagen H (2002) Atmospheric boundary layer monitoring at the meteorological observatory lindenberg as a part of the "Lindenberg column": facilities and selected results. Meteorol Z 11:241–253

Peltier LJ, Wyngaard JC (1995) Structure function parameters in the convective boundary layer from large-eddy simulation. J Atmos Sci 52:3641–3660

Raasch S, Schröter M (2001) PALM—a large-eddy simulation model performing on massively parallel computers. Meteorol Z 10:363–372

Roth M, Salmond JA, Satyanarayana ANV (2006) Methodological considerations regarding the measurement of turbulent fluxes in the urban roughness sublayer: the role of scintillometery. Boundary-Layer Meteorol 121:351–375

Spieß T, Bange J, Buschmann M, Vörsmann P (2007) First application of the meteorological mini-UAV M^2AV'. Meteorol Z 16:159–169

Tatarskii VI (1961) Wave propagation in a turbulent medium. McGraw-Hill Book Company Inc., New York, 285 pp

Thiermann V, Grassl H (1992) The measurement of turbulent surface-layer fluxes by use of bi-chromatic scintillation. Boundary-Layer Meteorol 58:367–389

van den Kroonenberg AC, Martin T, Buschmann M, Bange J, Vörsmann P (2008) Measuring the wind vector using the autonomous mini aerial vehicle M^2AV. J Atmos Ocean Technol 25:1969–1982

van den Kroonenberg AC, Martin S, Beyrich F, Bange J (2012) Spatially-averaged temperature structure parameter over a heterogeneous surface measured by an unmanned aerial vehicle. Boundary-Layer Meteorol 142:55–77

van Kesteren B, Hartogensis OK (2011) Analysis of the systematic errors found in the Kipp & Zonen large-aperture scintillometer. Boundary-Layer Meteorol 138:493–509

Von Randow C, Kruijt B, Holtslag AAM, de Oliveira MBL (2008) Exploring eddy-covariance and large-aperture scintillometer measurements in an Amazonian rain forest. Agric For Meteorol 148:680–690

Watts CJ, Chehbouni A, Rodriguez JC, Kerr YH, Hartogensis OK, De Bruin HAR (2000) Comparison of sensible heat flux estimates using AVHRR with scintillometer measurements over semi-arid grassland in northwest Mexico. Agric For Meteorol 105:81–89

Wesely ML (1976) The combined effect of temperature and humidity fluctuations on refractive index. J Appl Meteorol 15:43–49

Wyngaard J, Kosovic B (1994) Similarity of structure–function parameters in the stably stratified boundary layer. Boundary-Layer Meteorol 71:277–296

Wyngaard JC, Izumi Y, Collins SA (1971) Behavior of refractive-index structure parameter near ground. J Opt Soc Am 61:1646–1650